


RESEARCH ARTICLE

Comparative spatial transcriptomic profiling of severe acute respiratory syndrome coronavirus 2 Delta and Omicron variants infections in the lungs of cynomolgus macaques

Taehwan Oh¹ | Green Kim¹ | Seung Ho Baek¹ | YoungMin Woo^{1,2} |
Bon-Sang Koo¹ | Eun-Ha Hwang¹ | Kyuyoung Shim^{1,2} | You Jung An¹ |
Yujin Kim¹ | Jae-Hak Park³ | Jung Joo Hong^{1,2} 

¹Korea Research Institute of Bioscience and Biotechnology (KRIBB), National Primate Research Centre, Cheongju, Chungcheongbuk, Republic of Korea

²KRIBB School of Bioscience, Korea University of Science & Technology (UST), Daejeon, Republic of Korea

³Department of Laboratory Animal Medicine, College of Veterinary Medicine, Seoul National University, Seoul, Republic of Korea

Correspondence

Jung Joo Hong, Korea Research Institute of Bioscience and Biotechnology (KRIBB), National Primate Research Centre, 30, Yeongudanji-ro, Ochang-eup, Cheongwon-gu, Cheongju, Chungcheongbuk, Republic of Korea.
Email: hong75@kribb.re.kr

Funding information

Ministry of Science and ICT, South Korea, Grant/Award Number: NBS7952211; Korea Research Institute of Bioscience and Biotechnology (KRIBB) Research Initiative Programs, Grant/Award Number: KGM4572323; Korea Centers for Disease Control and Prevention, Grant/Award Number: 2020-ER5321-00

Abstract

Recently emerging severe acute respiratory syndrome coronavirus 2 (SARS-CoV-2) Omicron variants are generally less pathogenic than previous strains. However, elucidating the molecular basis for pulmonary immune response alterations is challenging owing to the virus's heterogeneous distribution within complex tissue structure. Here, we revealed the spatial transcriptomic profiles of pulmonary microstructures at the SARS-CoV-2 infection site in the nine cynomolgus macaques upon inoculation with the Delta and Omicron variants. Delta- and Omicron-infected lungs had upregulation of genes involved in inflammation, cytokine response, complement, cell damage, proliferation, and differentiation pathways. Depending on the tissue microstructures (alveoli, bronchioles, and blood vessels), there were differences in the types of significantly upregulated genes in each pathway. Notably, a limited number of genes involved in cytokine and cell damage response were differentially expressed between bronchioles of the Delta- and Omicron-infection groups. These results indicated that despite a significant antigenic shift in SARS-CoV-2, the host immune response mechanisms induced by the variants were relatively consistent, with limited transcriptional alterations observed only in large airways. This study may aid in understanding the pathogenesis of SARS-CoV-2 and developing a clinical strategy for addressing immune dysregulation by identifying potential transcriptional biomarkers within pulmonary microstructures during infection with emerging variants.

KEYWORDS

host immune response, nonhuman primates, pulmonary structure, SARS-CoV-2 variants, spatial transcriptomics

1 | INTRODUCTION

Coronavirus disease 2019 (COVID-19) was first reported in December 2019 and has spread rapidly since then, causing a pandemic. It is now in the process of entering an endemic phase worldwide.^{1,2} Severe acute respiratory syndrome coronavirus 2 (SARS-CoV-2), COVID-19's causative agent, is a zoonotic pathogen that continues to evolve in humans, generating variants with high transmissibility despite the rapid development of vaccines and antiviral agents.³ Several virus lineages have been classified as variants of concern (VOC) by the World Health Organization (WHO) based on their unusual and adverse impact on epidemiological and immunological characteristics. VOCs include Alpha, Beta, Gamma, Delta, and Omicron virus lineages, which have evolved to increase transmissibility and decrease pathogenicity.⁴ The risk of severe clinical outcomes following viral infection is lower in recently dominant Omicron variants than in existing ancestral variants, including Delta.^{5,6} Animal infection models have further confirmed that the pathogenicity of Omicron variants is lower than that of the early variants in hamsters, mice,^{7–9} and rhesus macaques.^{10,11}

The high transmissibility and low pathogenicity of Omicron variants are due to their variants replicating faster than other variants in the upper respiratory tract, such as the bronchi, but less efficiently in the lung parenchyma.^{12,13} Recent studies using single-cell RNA sequencing have revealed that the Omicron variant enter cells through a route different from that of other variants.¹⁴ Additionally, the Omicron variant induced a significantly lower level of inflammatory cytokines and chemokines than in the early variants.^{7,11} However, the methods established in previous studies are limited in that topological information is lost as the analyses used lung homogenates, nasosorption, or bronchoalveolar lavage samples. Analyses using these samples can reveal the global host response. However, they may not accurately reflect the local host response from viral target tissue architecture. This disadvantage is particularly highlighted because SARS-CoV-2 is non-uniformly distributed in respiratory tissues.¹⁵

Recent advances in spatial transcriptomics have enabled the investigation of transcriptional alterations in multiple cell types within complex tissue structures.¹⁶ Spatial transcriptomic analysis of lung tissues from humans infected with SARS-CoV-2 distinguished host responses in regions with and without viral RNA.¹⁷ Significant upregulation of genes related to inflammation, interferon (IFN) response, coagulation, and angiogenesis was observed in the virus-infected regions. Particularly, the genes related to the IFN response were preferentially expressed in the virus-positive site rather than a diffuse expression in the lung.¹⁸ Additionally, several genes related to the IFN pathway were upregulated in SARS-CoV-2-infected lungs compared to influenza-infected lungs, suggesting that spatially resolved transcriptomes can distinguish the specific profiles of one pathogen from another.^{15,18} Therefore, spatial transcriptomic analysis is suitable for confirming the interaction between a host and emerging pathogens at a molecular resolution without losing tissue structures.

SARS-CoV-2 pathogenesis is multifactorial by virus replication competence and dysregulated host innate immune responses. Thus, human patient-based assays are limited due to the heterogeneity between autopsy samples, such as individual pre-existing immunity. Also, all analyses of humans with COVID-19 used lung samples obtained at the end stage of the disease. Therefore, limitations exist in explaining the virus's pathogenesis and virulence at the disease induction stage. Nonhuman primates (NHP)—phylogenetically the closest animals to humans—are a valuable biological resource in that they provide opportunities to reveal the pathogenesis of emerging VOCs and evaluate next-generation vaccines and antivirals. We previously established NHP models experimentally infected with wild type and Delta variants of SARS-CoV-2, presenting the pathogens' virological, immunological, and pathological properties.^{19,20} This study employed whole spatial transcriptome analysis to compare the transcriptional changes in the host response between SARS-CoV-2 variant infections in macaque lungs. Conventional histopathological examinations were also performed on the pulmonary structures, including the alveoli, bronchioles, and blood vessels. This represents the first investigation to compare host response transcriptional alterations between Omicron and Delta variants of SARS-CoV-2 in pulmonary microstructures.

2 | MATERIALS AND METHODS

2.1 | Experimental design

Comparative analysis of SARS-CoV-2 variants was performed in Cambodian-origin cynomolgus macaques (*Macaca fascicularis*) experimentally infected with Delta (NCCP. 43390 for the GK clade [B.1.617.2 lineage]) and Omicron (NCCP. 43408 for the GRA clade [B.1.1.529 lineage]) variants. Three female 3–6-year-old macaques in each experimental group were inoculated with 2.1×10^6 50% tissue culture infectious doses/mL ([TCID₅₀]/mL) of the virus in 12.5 mL via multiple routes (intratracheal, oral, conjunctival, intranasal, and intravenous).^{19,20} The mock-infected group was inoculated with the same volume of PBS via the same route. Macaques were euthanized and necropsied 3 days postinfection (dpi), and respiratory organs were collected.

2.2 | Histopathology

The lung lesions from the six lobes (right upper, middle, and lower and left upper, middle, and lower) were classified into four grades: Grade 1, alveolar wall thickening with Type II pneumocyte hyperplasia and mononuclear cell infiltration but intact vascular endothelium; Grade 2, alveolar wall thickening and vascular endothelial damage with neutrophil and mononuclear cell infiltration; Grade 3, alveolar edema, alveolar wall thickening, and vascular endothelial damage; Grade 4, hyaline membrane formation, alveolar edema, alveolar wall thickening, and vascular endothelial damage. The prevalence of the

lesions from the six lobes was also evaluated at three levels: Stage 1, <30%; Stage 2, 30–<50%; Stage 3, >50% of the total tissue section's area. Two pathologists blindly estimated the grade.

2.3 | Immunohistochemistry

Antigen distribution in lung tissue sections from infected macaques was confirmed via immunohistochemistry (IHC). IHC procedures followed a previously described method with slight modifications.^{19,20} The slides were visualized using 3,3-diaminobenzidine (DAB), followed by counterstaining with hematoxylin. The antigen score was semiquantitative as described previously²¹: 3(+++), extensive antigen; 2(++), moderate antigen; 1(+), occasional or minimal antigen; and 0(–), negative for antigen. Two pathologists blindly estimated the score.

2.4 | Tissue morphology

The lung sections were characterized using immunohistochemical staining for combined epithelial cell marker—PanCK (Novus, Clone AE1 + AE3), immune cell marker—CD45 (Novus, Clone 2B11+PD7/26), and macrophage marker—CD68 (Santa Cruz, Clone KP1) along with Syto13 DNA nucleic acid staining. CD68 was quantified in lung sections (10 image fields per macaque, $n = 90$) using Image J (National Institutes of Health) histogram analysis with an inverted 16-bit.

2.5 | GeoMx digital spatial profiling (DSP) for whole transcriptome analysis (WTA)

NanoString GeoMx was used for the spatial transcriptomic analysis of lung tissues from experimentally infected animals, as previously described.^{22–24} We prepared 4 μ m FFPE (formalin-fixed paraffin embedded) tissue sections from Delta and Omicron variants- and mock-infected animals. The tissue slides were hybridized with probes for the Human Whole Transcriptome Atlas targeting >18 000 genes and then tissue morphology was visualized using immunofluorescence for PanCK, CD45, and CD68 with Syto13 DNA nucleic acid staining. Thereafter, the slides were loaded onto the GeoMx Digital Spatial Profiler (DSP) and then region of interest (ROI) selection was guided using IHC staining of the nucleocapsid of the virus in serial sections. Photo-cleaving UV light (385 nm) was projected onto the selected ROI to release and collect the oligos using a microcapillary, which were deposited in a 96-well plate. The deposited photo-cleaved indexing oligos were dried overnight and resuspended in diethyl pyrocarbonate-treated water. Sequencing libraries were constructed and pooled libraries were sequenced using Illumina NovaSeq. 6000 following the manufacturer's protocol. Quality-controlled sequencing data were generated and further processed to quantify RNA expression digitally.

2.6 | Bioinformatics

Before downstream analysis, each ROI's data were scaled to have the same 75th percentile (quartile 3; Q3) of the RNA expression signal, a generally preferred normalization strategy for WTA data. Briefly, gene counts' Q3 for each ROI was estimated and normalized to the geometric mean of the Q3 across all ROIs. Q3 normalized counts were then transformed to log2 values and used for the analysis.

Dimensionality reduction was performed using principal component analysis (PCA) to identify important trends and patterns in gene expression datasets according to the experimental design. The analysis captured the orthogonal dimensions of the data set's variability, simplifying the complexity of high-dimensional data by converting the data into lower dimensions. The analysis was performed using the R package provided by NanoString.

Differentially expressed genes (DEGs) between each experimental group passed the filters of Benjamini–Hochberg adjusted $p < 0.05$ and absolute log₂ fold change >1. Gene set enrichment analysis (GSEA) identified the gene set significantly related to specific pathways in the sequencing data of virus- and mock-infected groups. The analysis was performed using the GSEA 4.2.3 software package with the “HALLMARK” gene set collections (50 sets) obtained from the molecular signatures database (MSigDB version 7.1). Normalized enrichment score (NES) accounting for the size of each gene set was estimated, and a false discovery rate (FDR) < 0.05 (5E-2) was assessed as significant enrichment.

Cell deconvolution of gene expression data was performed to estimate the abundance of mixed cells in each ROI from the experimental groups. The analysis was performed using the Spatial-Decon R package version 1.2. The algorithm script was derived from the cell profile library of the Human Cell Atlas adult lung.²⁵

3 | RESULTS

3.1 | Decreased pathology of the Omicron variant compared to the Delta variant in the cynomolgus macaque model

In the four histopathological grading systems, the Delta-infected group had a significantly higher grade than the Omicron-infected group (Figure 1A,E). Both groups had alveolar edema or hyaline membrane formation in three lung lobes, indicating severe damage to the lung parenchyma. Prevalence scores were evaluated based on the lesion size at three levels. There were no significant differences in the prevalence scores between the Delta- and Omicron-infected groups (Figure 1B,E). Prevalence scores varied according to lung lobe; both groups had extensive lesion distribution (>50% of the total tissue section) in one lobe. IHC analysis revealed a nonsignificant trend toward higher antigen scores in the Delta-infected macaques than in the Omicron-infected macaques

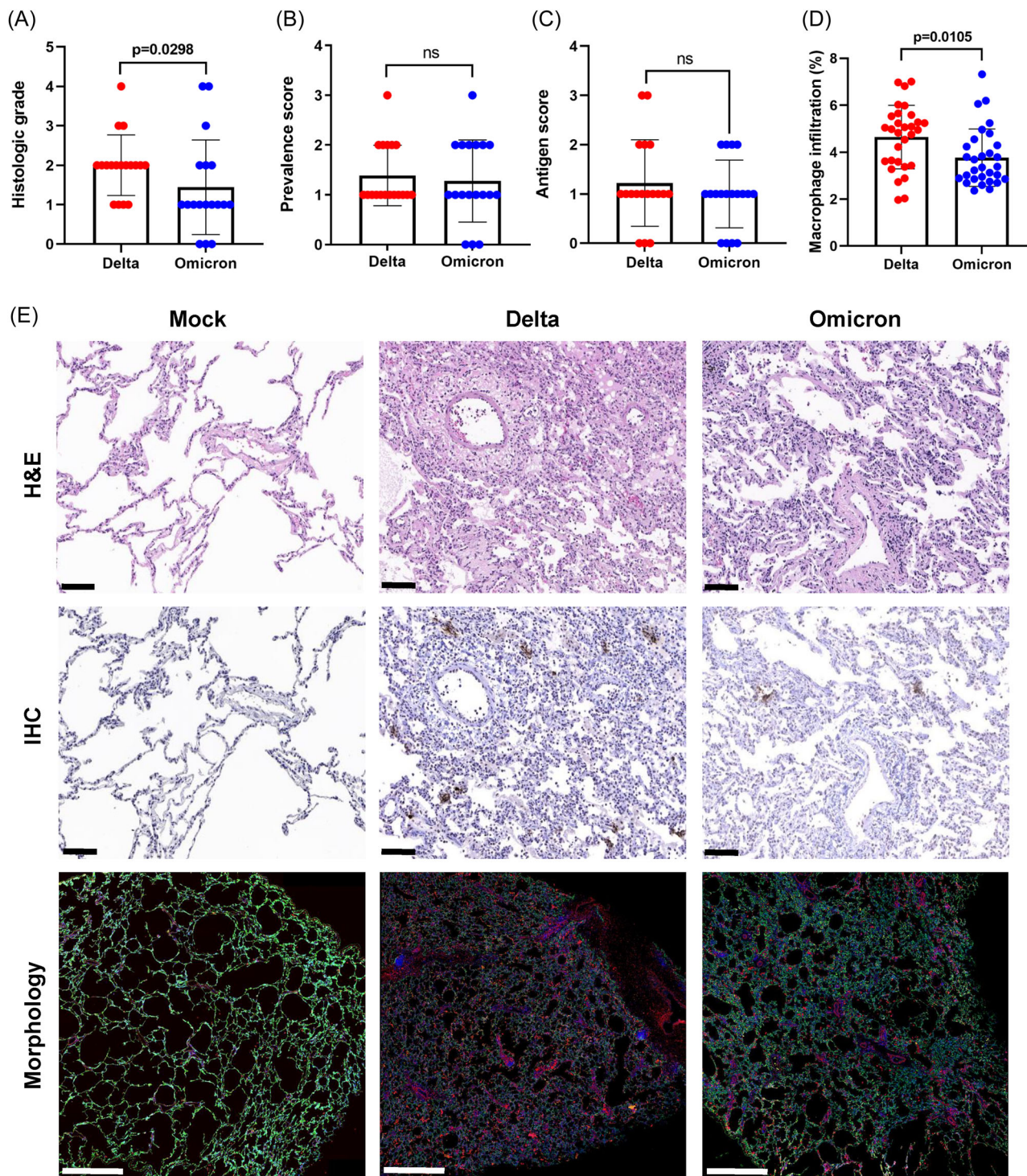


FIGURE 1 Pathological examination of SARS-CoV-2 Delta and Omicron variants. Histologic grade (A), prevalence score (B), viral antigen score (C), and macrophage infiltration (D) of left and right lung lobes (upper/middle/lower) in Delta- and Omicron-infected macaques necropsied at 3 dpi. Significant differences were indicated in the *p* value between the macaque groups. The representative figure of histopathology, immunohistochemistry, and morphology in Delta- and Omicron-infected macaques (E). Hematoxylin and eosin (H&E) indicates H&E staining. Scale bar, 100 μ m. Immunohistochemistry (IHC) indicates DAB-labeling (brown) immunohistochemistry for viral nucleic acid. Scale bar, 100 μ m. Morphology indicates tissues visualized with epithelial cell marker—PanCK (green), immune cell marker—CD45 (yellow), and macrophage marker—CD68 (red) with Syto13 DNA nucleic acid (blue) staining. Scale bar, 1000 μ m.

(Figure 1C,E). The Delta-infected group had moderate and extensive amounts of viral antigens in three and two lung lobes, respectively. The Omicron-infected group had a moderate amount of viral antigens in four lung lobes. Macrophage infiltration was quantified by evaluating the signal intensity of CD68. The percentage of positive areas was significantly higher in the Delta-infected group ($4.64 \pm 1.35\%$) than in the Omicron-infected group ($3.76 \pm 1.22\%$) (Figure 1D,E). The area % of CD68 varied among the different lung lobes; however, the Delta- and Omicron-infected groups displayed widespread macrophage infiltration.

3.2 | ROI selection for comparative spatial transcriptomic analysis

In total, 108 ROIs representing three morphological sites from 9 macaques (alveolar (36), bronchiolar (36), and vascular (36) ROIs; 12 ROIs per experimental group) were chosen by veterinary pathologists (Figure 2A). Selecting alveolar and bronchiolar ROIs was easily guided via IHC staining of the viral antigens on serial section slides. However, the vascular ROIs were adjacent to other structural ROIs because they had lower sensitivity for IHC

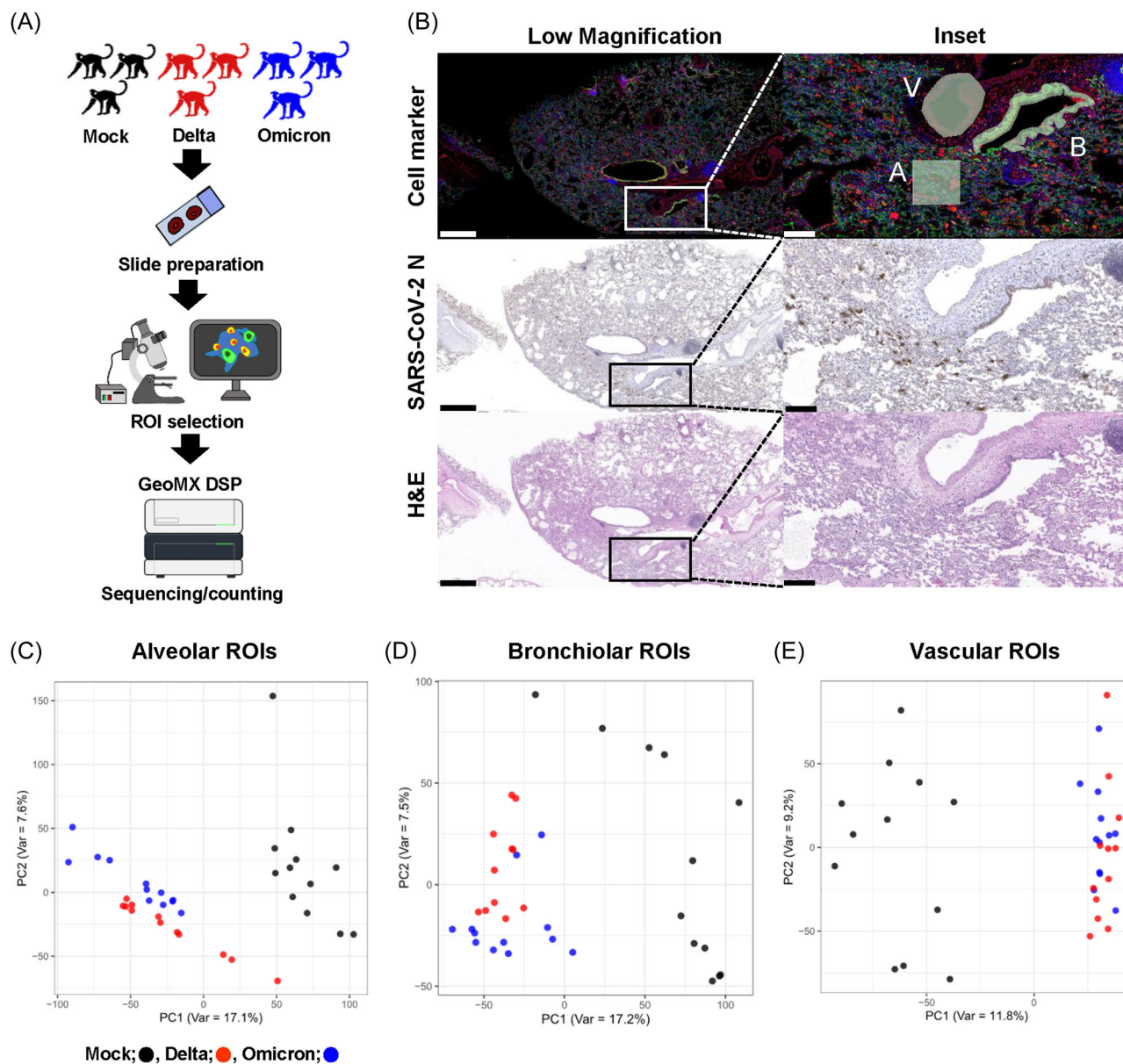


FIGURE 2 Schematic design of the study and exploratory analysis of the spatial transcriptome. (A) Experimental design of GeoMx digital spatial profiling. (B) Strategy of the region of interest (ROI) selection. Tissue architectures were annotated as A, alveolar; B, bronchiolar; V, vascular ROIs. Immunohistochemistry indicates DAB-labeling (brown) immunohistochemistry for SARS-CoV-2 viral nucleic acid (N). H&E indicates hematoxylin and eosin staining. Scale bar, low magnification; 1000 μ m and inset; 200 μ m. PCA plots of alveolar (C), bronchiolar (D), and vascular (E) ROIs are shown. Graphs represent all ROIs selected from the Delta, Omicron, and mock-infected macaque groups.

(Figure 2B). Histopathology (histologic grade/prevalence score/viral antigen score) for lung lobes containing each structural ROIs were presented in Table 1. Delta-infected ROIs were selected from lung lobes with Grade 2, Stage 1–2, and antigen score 1–3. Omicron-infected ROIs were selected from lung lobes with Grade 1–2, Stage 1–2, and antigen score 1–2. Mock-infected ROIs were selected from intact lung lobes that were all antigen negative.

3.3 | Dimensionality reduction in the spatial transcriptomic data set of Delta and Omicron infections

PCA of the spatial transcriptomic data was conducted to explore the variation in Delta-, Omicron-, and mock-infected lung specimens. PCA ruled out the individual (macaque) differences and experimental (GeoMX scan) batch variations. The virus-infected alveolar ROIs were separated from the mock-infected alveolar ROIs in the PCA of transcriptomic data, and the ROIs from the Delta- and Omicron-infected lungs clustered. In PCA of transcriptomic data from bronchiolar and vascular ROIs, Delta- and Omicron-infected ROIs overlapped substantially. These results suggest that the spatial transcriptomic profiles of Delta- and Omicron-infected lungs did not vary significantly (Figure 2C–E).

3.4 | Spatial transcriptomic profile of host response to Delta and Omicron infection in alveoli

Compared to mock-infected lungs, Delta- and Omicron-infected lungs exhibited 329 and 121 significantly co-upregulated and

co-downregulated genes, respectively, in the alveolar ROIs. No contra-regulated genes were observed between Delta- or Omicron-infected alveoli and mock-infected alveoli. Significantly upregulated and downregulated genes were enriched in the inflammation/response to pathogen, complement/cell death and damage, and proliferation/activation/differentiation pathways, displaying similar patterns of gene expression between Delta- and Omicron-infected alveolar ROIs (Figure 3A). The genes involved in each pathway are listed in Supporting Information: Tables 1–3.

GSEA displayed significant enrichment of gene sets, including inflammatory response, IFN alpha response, IFN gamma response, TNF-alpha (TNFA) signaling via NFkB, interleukin (IL)-2 STAT5 signaling, IL-6 JAK-STAT3 signaling, complement, apoptosis, hypoxia, reactive oxygen species, P53, mitotic spindle, glycolysis, and oxidative phosphorylation pathways in Delta- or Omicron-infected alveoli. Additionally, the gene sets were significantly enriched, including coagulation and epithelial/mesenchymal transition pathways, in Delta-infected alveoli (Figure 3B). GSEA revealed no significant differences in the gene sets between Delta- and Omicron-infected alveoli.

Differences in single gene expression between Delta- and Omicron-infected groups were limited, and only TFPI2 gene (involved in coagulation and the complement pathway) was upregulated in the alveolar ROIs of the Delta-infected group compared to those of the Omicron-infected group (Figure 3C and Supporting Information: Figure 1).

Cell deconvolution analysis revealed that the proportion of B, plasmacytoid dendritic, macrophage, and CD8+ cytotoxic T cells was significantly higher in Delta- and Omicron-infected alveolar ROIs than in mock-infected ROIs. Additionally, significant increase of NK cell proportion was observed in delta-infected ROIs compared to

TABLE 1 Histopathologic scoring for lung lobes containing alveolar, bronchiolar, and vascular ROIs.

	Alveolar ROIs			Bronchiolar ROIs			Vascular ROIs		
	Delta	Omicron	Mock	Delta	Omicron	Mock	Delta	Omicron	Mock
ROI#1	2/2/2	1/2/1	0/0/0	2/2/2	1/2/1	0/0/0	2/2/2	1/2/1	0/0/0
ROI#2	2/2/2	1/2/1	0/0/0	2/2/2	1/2/1	0/0/0	2/2/2	1/2/1	0/0/0
ROI#3	2/2/2	1/1/1	0/0/0	2/2/2	1/2/1	0/0/0	2/1/1	1/2/1	0/0/0
ROI#4	2/2/2	1/1/1	0/0/0	2/2/2	1/2/1	0/0/0	2/2/2	1/2/1	0/0/0
ROI#5	2/2/2	1/1/1	1/1/0	2/1/3	1/1/1	1/1/0	2/2/2	1/1/1	1/1/0
ROI#6	2/2/2	1/1/1	1/1/0	2/1/3	1/1/1	1/1/0	2/1/1	1/1/1	1/1/0
ROI#7	2/1/3	2/2/2	1/1/0	2/2/2	1/1/1	1/1/0	2/1/1	1/1/1	1/1/0
ROI#8	2/1/3	2/2/2	1/1/0	2/2/2	1/1/1	1/1/0	2/1/1	1/1/1	1/1/0
ROI#9	2/1/1	1/2/1	0/0/0	2/1/1	2/2/2	0/0/0	2/1/1	2/2/2	0/0/0
ROI#10	2/1/1	1/2/1	0/0/0	2/1/1	2/2/2	0/0/0	2/1/3	2/2/2	0/0/0
ROI#11	2/2/2	2/2/2	0/0/0	2/2/2	2/2/2	0/0/0	2/1/3	2/2/2	0/0/0
ROI#12	2/1/1	2/2/2	0/0/0	2/2/2	2/2/2	0/0/0	2/2/2	2/2/2	0/0/0

Note: Results for each structural ROI in Delta, Omicron, and mock-infected groups were shown as histologic grade/prevalence score/viral antigen score. Abbreviation: ROI, region of interest.

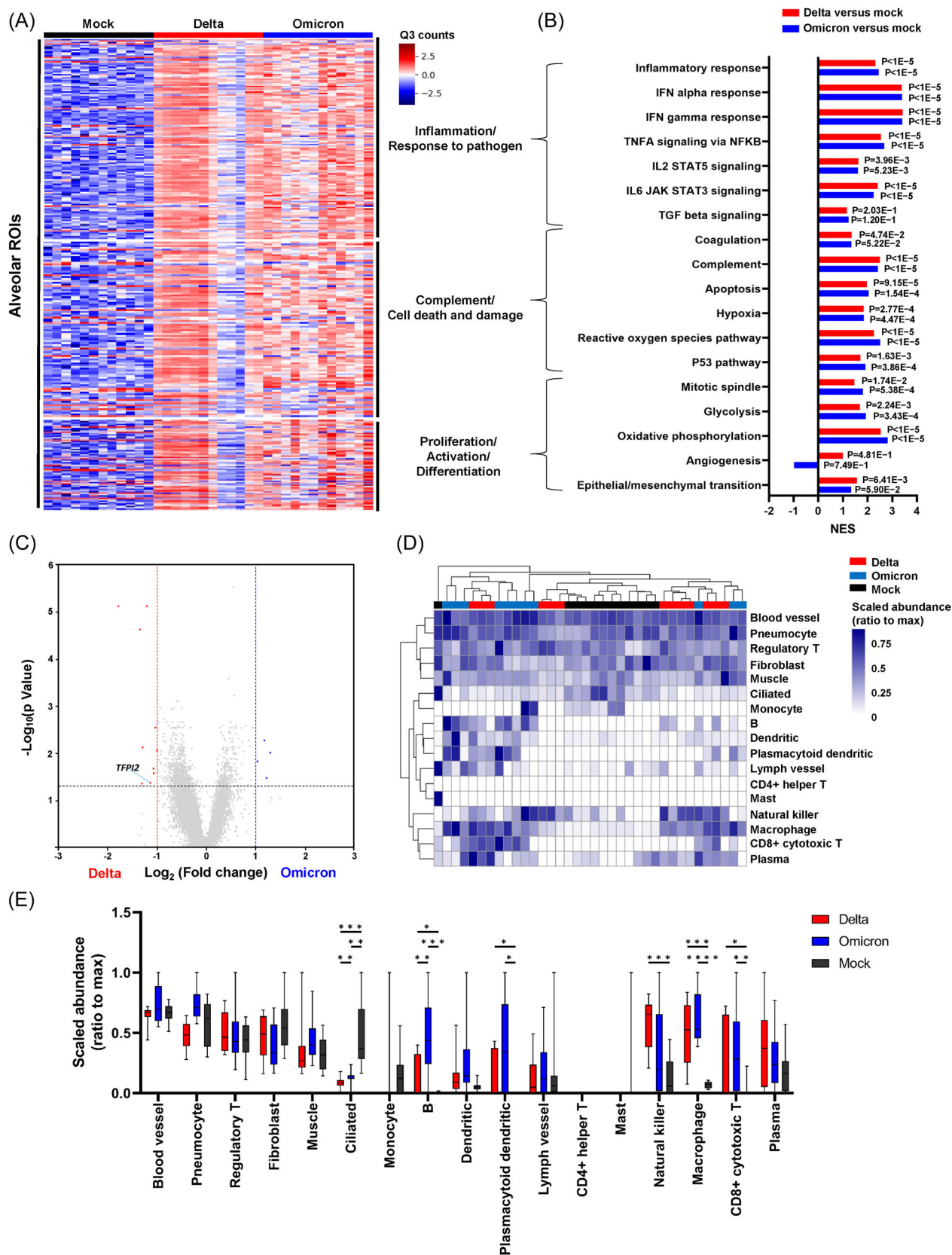


FIGURE 3 (See caption on next page)

mock-infected ROIs. In mock-infected ROIs, the proportion of ciliated cells was significantly higher compared to Delta and Omicron-infected ROIs (Figure 3D,E).

3.5 | Spatial transcriptomic profile of host response to Delta and Omicron infection in bronchiole

Compared to mock-infected lungs, Delta- and Omicron-infected lungs exhibited 483 and 220 significantly co-upregulated and co-downregulated genes, respectively, in the bronchiolar ROIs. No contra-regulated genes were observed between Delta- or Omicron-infected bronchioles and mock-infected bronchioles. Significantly upregulated and downregulated genes were enriched in the inflammation/response to pathogen, complement/cell death and damage, and proliferation/activation/differentiation pathways, with similar patterns of gene expression between Delta- and Omicron-infected bronchiolar ROIs (Figure 4A). The genes involved in each pathway are listed in Supplementary Tables 4–6.

GSEA revealed significant enrichment of gene sets in pathways including inflammatory response, IFN alpha response, IFN gamma response, TNFA signaling via NFKB, IL2 STAT5 signaling, IL6 JAK STAT3 signaling, TGF beta signaling, complement, apoptosis, hypoxia, reactive oxygen species, P53, mitotic spindle, glycolysis, and oxidative phosphorylation pathways in Delta- or Omicron-infected bronchioles. Additionally, gene sets were significantly enriched in the coagulation pathway in Delta-infected bronchioles and angiogenesis and epithelial/mesenchymal transition pathway in Omicron-infected bronchioles (Figure 4B). GSEA revealed no significant differences in the gene sets between Delta- and Omicron-infected bronchioles.

In bronchiolar ROIs, differential transcriptomes of several pathway genes were identified between the Delta- and Omicron-infected groups, upregulating HLA-G (related to interferon-gamma response), HK2 (IL2 STAT5 signaling), ANXA1 and GSN (related to apoptosis and coagulation), HMGB2 (related to apoptosis), F3 (related to inflammatory response and complement), CA12, IGFBP3, and PKP1 (related to hypoxia), ITGB4, PERP, and SERPINB5 (related to the P53 pathway), LMNB1 (related to mitotic spindle), STMN1 (related to glycolysis), and MCM7 (related to epithelial-mesenchymal transition) in Delta-infected groups. It also upregulated FBP1 (related to hypoxia), GPX3 (related to apoptosis), and CAT (reactive oxygen species) in the Omicron-infected groups (Figure 4C and Supporting Information: Figure 1).

Cell deconvolution analysis revealed that the proportion of macrophages and pneumocytes was significantly higher in Delta- and Omicron-infected bronchiolar ROIs than in mock-infected ROIs. Also, significant increase of fibroblast and regulatory T cell proportions was observed in omicron-infected ROIs compared to Delta- and mock-infected ROIs (Figure 4D,E).

3.6 | Spatial transcriptomic profile of host response to Delta and Omicron infection in blood vessel

Compared to mock-infected lungs, Delta- and Omicron-infected lungs exhibited 134 and 43 significantly co-upregulated and co-downregulated genes, respectively, in the vascular ROIs. No contra-regulated genes were observed between Delta- or Omicron-infected blood vessels and mock-infected blood vessels. Significantly upregulated and downregulated genes were enriched in the inflammation/response to pathogen, complement/cell death and damage, and proliferation/activation/differentiation pathways, with similar patterns of gene expression between Delta- and Omicron-infected vascular ROIs (Figure 5A). The genes involved in each pathway are listed in Supporting Information: Tables 7–9.

GSEA uncovered significant enrichment of gene sets, including inflammatory response, IFN alpha response, IFN gamma response, TNFA signaling via NFKB, IL6 JAK STAT3 signaling, and oxidative phosphorylation pathway in Delta- or Omicron-infected blood vessels. Additionally, gene sets, including IL2 STAT5 signaling, TGF beta signaling, complement, apoptosis, hypoxia, reactive oxygen species, P53 pathway, mitotic spindle, glycolysis, and angiogenesis, were elevated in Delta- and Omicron-infected blood vessels, albeit not significantly in Delta-infected blood vessels (Figure 5B). GSEA revealed no significant difference in the gene sets between Delta- and Omicron-infected blood vessels. Also, there were no significant differences in single gene expression existed between the Delta- and Omicron-infected vascular ROIs (Figure 5C).

Cell deconvolution analysis revealed that the proportion of macrophages was significantly higher in Delta- and Omicron-infected vascular ROIs than in mock-infected ROIs. Additionally, significant increase of regulatory T cell proportion was observed in omicron-infected ROIs compared to mock-infected ROIs. There were no distinguishable variation in the patterns of inflammatory cell infiltration between Delta and Omicron infections in the blood vessel of the lung (Figure 5D,E).

FIGURE 3 Spatial transcriptomic analysis in alveolar regions of interest (ROIs) from mock-, Delta-, and Omicron-infected lungs. (A) Heat maps were shown for differential expression genes (DEGs) obtained by comparing Q3 normalized counts between alveolar ROIs in Delta and Omicron-infected lungs versus mock-infected lungs. (B) normalized enrichment scores (NES) and adjusted *p* values obtained by gene set enrichment analysis (GSEA) were shown for alveolar ROIs in Delta- and Omicron-infected lungs versus mock-infected lungs. (C) Volcano plots were shown for major differential expression genes (DEGs) between alveolar ROIs of the Delta- and Omicron-infection groups. (D) Heat map of cell deconvolution data in Delta-, Omicron-, and mock-infected alveolar ROIs. Results were presented for the abundance of mixed cell types in the ROIs, and scaled abundance was presented as a ratio to the max. (E) Box plots of cell deconvolution data. *****p* < 0.0001; ****p* < 0.001; ***p* < 0.01; **p* < 0.05, ANOVA, pairwise comparisons between groups, Benjamini–Hochberg FDR adjustment.

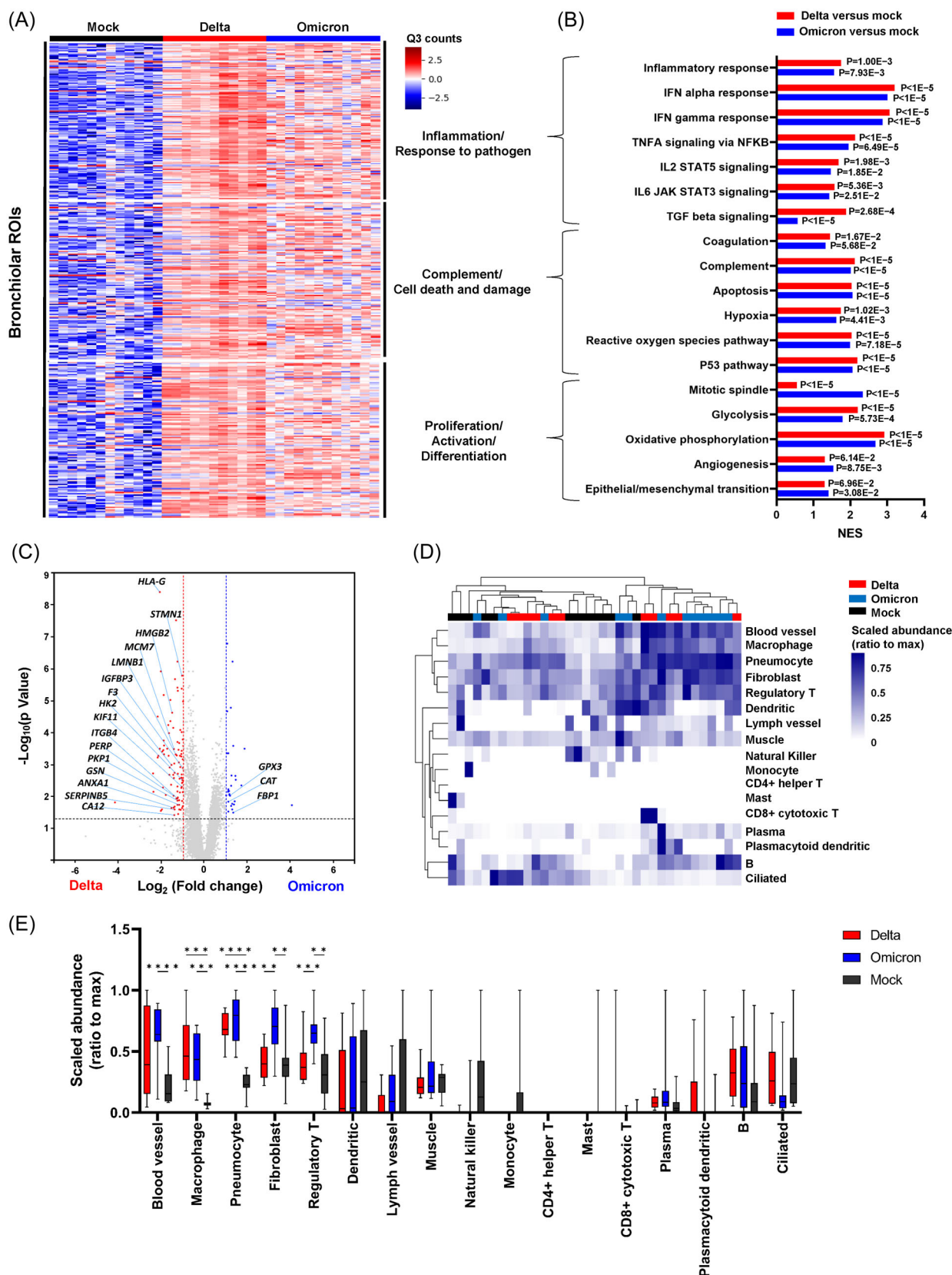


FIGURE 4 (See caption on next page)

4 | DISCUSSION

Consistent with previous macaque model studies,^{10,11} our conventional histopathological examination revealed lower virulence of the Omicron variant than that of the Delta variant in cynomolgus macaques. Previous infection studies using rhesus macaques have explained the lower disease severity of Omicron, with significantly lower viral loads in nasal and bronchial swab samples and lung tissues and the lower regulation of cytokines and chemokines in nasosorption samples, than that of Delta-infected animals.¹¹ Directly quantifying cytokines and chemokines or measuring the expression levels of immune-related genes via RNA sequencing can obtain a global overview of host responses throughout the tissue. However, lesion and antigen distribution is not uniform within SARS-CoV-2-infected lungs. Thus, the host's response to the virus has a high level of intrapulmonary spatial heterogeneity.¹⁸ These issues emphasize the need for spatial transcriptome techniques in analyzing the pathogenesis of emerging SARS-CoV-2 variants. In a previous spatial transcriptome study,¹⁵ the most distinct biological factor was the dominant cell type in each tissue type. Therefore, in this study, the target region of the transcriptomic analyses comprised the three most distinct structures in the lung: the alveoli, bronchioles, and blood vessels.

PCA is routinely used to interpret spatial transcriptomes,¹⁵ which can identify important trends and patterns of gene expression data. This simplifies the complexity of high-dimensional data by converting them into lower dimensions. Gene expression data of Delta- or Omicron-infected lungs were separated from those of noninfected lungs; however, they overlapped in the PCA plot of all three structures of the ROIs. Consistent with the PCA results, DEG analysis and GSEA confirmed that the spatial transcriptomic profiles of the Delta- and Omicron-infected lungs did not significantly vary. Previous host transcriptomic analyses have displayed a significant upregulation of genes related to inflammation, IFN- α and IFN- γ responses, IL2 STAT5, IL6 JAK STAT3, and TNF- α signaling, coagulation, complement, angiogenesis, and epithelial/mesenchymal transition in lungs from SARS-CoV-2-infected human patients compared to lungs from nonviral deaths.^{15,26} Recent studies in mice infected with the MA10 strain virus confirmed the transcriptomic profiles of acute and chronic host responses similar to those observed in humans with COVID-19.²⁴ Here, we demonstrated that SARS-CoV-2 Delta- and Omicron-variant-infected macaques have a transcriptomic host response profile similar to that

of human patients and previous mouse models. Moreso, it is characterized by upregulated gene pathways involved in inflammation, cytokine response, complement, cell damage, proliferation, and differentiation.

We identified notable changes in the cell population of the three structural ROIs, particularly in the alveolar ROIs, between the mock- and virus-infected lungs. In the cell deconvolution analysis, Delta- and Omicron-infected alveoli had a relatively high proportion of inflammatory cells, including macrophages, NK cells, and T cells. This is consistent with the findings of DEG analysis, which revealed that the enhanced expression of macrophage cell markers (CD163, CD68, CYBB, FUCA1, GPNMB, LGMN) and loss of AT1 cell markers (AGER, HOPX, CAV1) and AT2 cell markers (ABCA3, LAMP3, SFTPB, SFTPC) in the Delta- and Omicron-infected ROIs. This is consistent with previous reports that virus-infected regions have increased heterogeneity in cell populations with significantly decreased AT2 cells and increased macrophages, fibroblasts, and endothelial cells.^{17,27} This is also in line with previous human autopsy data¹⁸ and mice model data,²⁴ wherein early loss of surfactant protein genes was observed in diseased alveoli. These results can explain the upregulated inflammation and cytokine pathways concurrent with downregulated surfactant metabolism in the virus-infected ROIs. Furthermore, we found that fibroblast and regulatory T cells were significantly increased in omicron-infected bronchiolar ROIs, suggesting that the enhanced transcriptomic alterations were induced in the related functional gene pathways.

Cytokine release syndrome plays a critical role in the clinical outcomes of severe COVID-19. Once the virus is detected by the pathogen recognition mechanism, the production of Type 1 and Type 3 IFNs is stimulated, and interferon-stimulating genes (ISGs) are expressed via the JAK-STAT signaling pathway. In this macaque infection model, ISGs were co-upregulated in alveolar (ISG15 and ISG20), bronchiolar (ISG15), and vascular (ISG15) ROIs in Delta- and Omicron-infected groups. Nonetheless, no significant difference was noted between both groups. Some ISGs were higher in each tissue structure, corroborating with a previous mouse report that the ISG expression patterns of the large airway and alveolar ROIs did not match.²⁴ Significantly higher expression of STAT1 and STAT2 was observed in Delta- and Omicron-infected lungs than in mock-infected lungs, as observed in ROIs with high viral titers compared to that in ROIs with low viral titers in human patients.¹⁸ Clinical trials have been conducted to reduce the cytokine storm by regulating intracellular signaling mediated by the JAK/STAT pathway.²⁸

FIGURE 4 Spatial transcriptomic analysis in bronchiolar region of interests (ROIs) from mock-, Delta-, and Omicron-infected lungs. (A) Heat maps were illustrated for differential expression genes (DEG) obtained by comparing Q3 normalized counts between bronchiolar ROIs in Delta- and Omicron-infected lungs versus mock-infected lungs. (B) Normalized enrichment scores (NES) and adjusted *p* values obtained by gene set enrichment analysis (GSEA) were shown for bronchiolar ROIs in Delta- and Omicron-infected lungs versus mock-infected lungs. (C) Volcano plots were shown for major differential expression genes (DEGs) between bronchiolar ROIs of the Delta- and Omicron-infection groups. (D) Heat map of cell deconvolution data in Delta-, Omicron-, and mock-infected bronchiolar ROIs. Results were presented for the abundance of mixed cell types in the ROIs, and scaled abundance was presented as a ratio to the max. (E) Box plots of cell deconvolution data. *****p* < 0.0001; ****p* < 0.001; ***p* < 0.01; **p* < 0.05, ANOVA, pairwise comparisons between groups, Benjamini-Hochberg FDR adjustment.

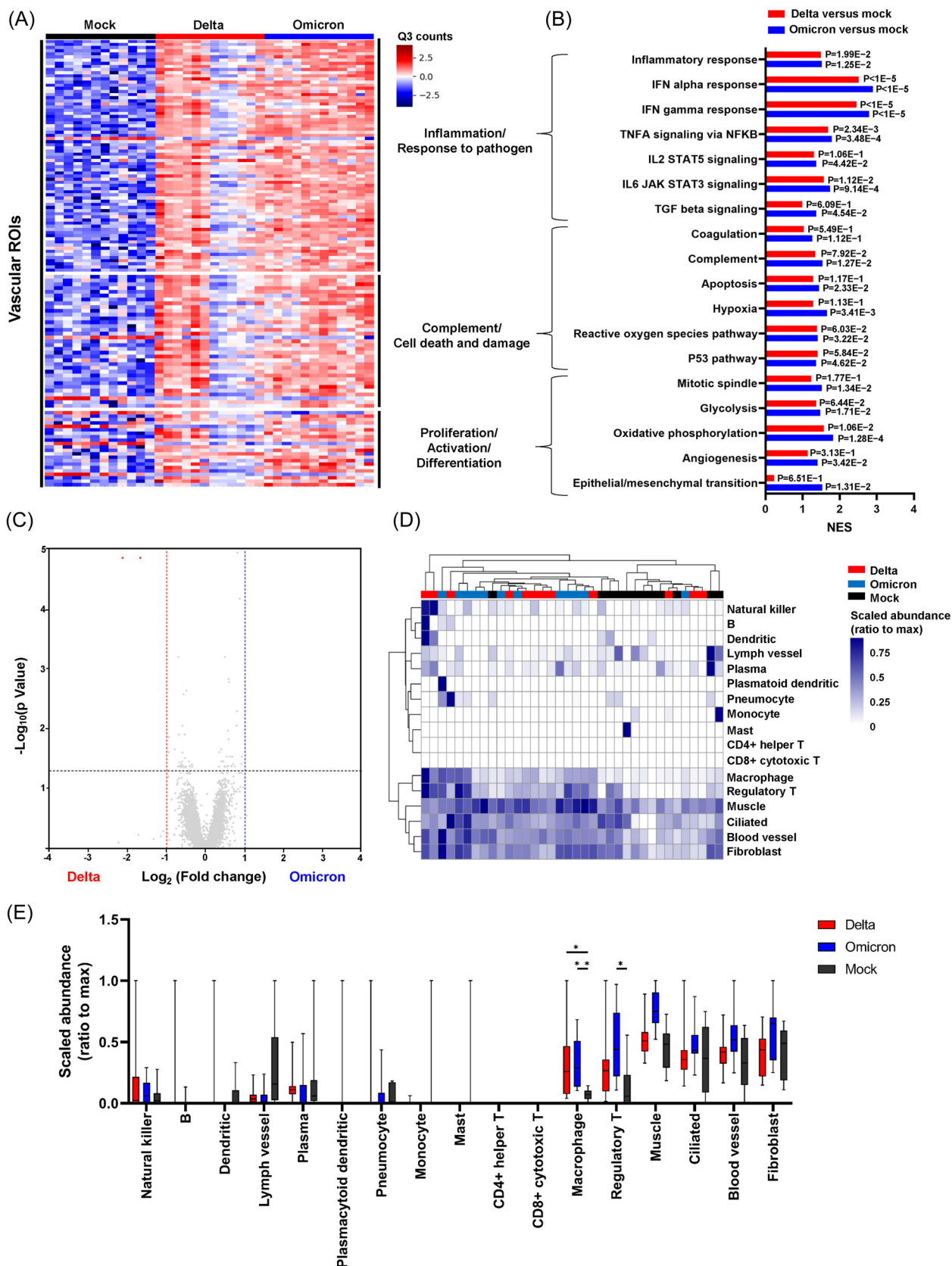


FIGURE 5 (See caption on next page)

Our results revealed that the host immune response to Delta and Omicron infections was comparable across the three lung tissue structures, suggesting that a common immune regulation approach may apply to infections caused by SARS-CoV-2 variants.

Next, we focused on genes previously identified as hallmarks of severe SARS-CoV-2 infection. IFI27 is a proposed biomarker for the high risk of SARS-CoV-2 infection in the early COVID-19 phase in blood samples²⁹ and discriminating SARS-CoV-2 infection from influenza infection in lung samples.¹⁵ It had significant expression enrichment in all three structural ROIs from the Delta- and Omicron-infected lungs. S100/Calbindin genes, such as S100A4, S100A6, S100A8, and S100A9, which play a direct role in recruiting leukocytes to infected cells, have been proposed as potential biomarkers that can distinguish between mild and severe COVID-19 progressions.^{30,31} There was a significant increase in S100A9 in bronchiolar ROIs of Delta- and Omicron-infected lungs, without differential expression between lungs infected with both variants. THBS1, which is involved in the platelet activation-related pathway, was upregulated in fatal COVID-19 cases compared to moderate cases.³² Delta- and Omicron-infected lungs had significant gene enrichment in alveolar ROIs. These results suggested that both SARS-CoV-2 variants represent severe disease progression in macaques at an early infection stage. In addition, the expression patterns of known biomarker genes differed for each tissue microstructure.

We additionally performed a comparative analysis of the viral entry genes potentially associated with SARS-CoV-2 infectivity, including angiotensin-converting enzyme 2 (ACE-2), transmembrane serine protease 2 (TMPRSS2), and basigin (BSG/CD147). Generally, the viral surface spike glycoprotein binds to ACE2 receptors to allow viral entry into cells.³³ No significant difference in the expression level of the ACE2 gene was observed between Delta- or Omicron-infected groups and mock-infected groups for all three tissue structures of the ROIs. Recently, TMPRSS2 was found to support cell surface/early endosomal entry of SARS-CoV-2,³⁴ and the Delta variant is more dependent on this entry pathway than Omicron variants.¹⁴ TMPRSS2 revealed significantly higher expressions in Delta- and Omicron-infected bronchiolar ROIs than in mock-infected bronchiolar ROIs, albeit with a lower log2 fold change (0.963 and 0.857, respectively). Recently identified as another host receptor,^{35,36} BSG (CD147) had the highest average expression levels among viral entry genes. BSG was significantly co-upregulated in Delta- and Omicron-infected lungs compared to mock-infected lungs in alveolar ROIs (log2fold change 0.584 and 1.005, respectively) and

bronchiolar ROIs (log2fold change 0.955 and 0.946, respectively). This was consistent with previous studies revealing that BSG (CD147) had the highest mean expression levels, and ACE2 was the lowest, with frequent undetectable levels among viral entry genes of lung samples in patients with COVID-19.¹⁸ In the present study, we confirmed that the expression patterns of genes involved in viral entry differed according to tissue structures. Furthermore, no difference in gene expression existed between the Delta- and Omicron-infected groups in all three tissue structures of the ROIs at early phase of infection.

Although GSEA did not yield a significant differential gene set pathway between Delta- and Omicron-infected lungs in all three structures of ROIs, there was a slight difference in single gene expression pattern in the DEG analysis. We designated these DEGs as differential transcriptional signatures in Delta versus Omicron infection. In the alveolar region, we observed significant upregulation of tissue factor pathway inhibitor-2 (TFPI2) gene in Delta infections. TFPI2 inhibits serine proteases, including the tissue factor-VIIa complex, thus suppressing thrombin generation.³⁷ However, its upregulation also indicates the activation of counteractive mechanism that inhibits overt coagulation cascade.³⁸ We have identified the potential of this gene as an indicator of aggravated coagulation cascade in alveolar microvascular complications. In the bronchiolar regions, differential transcriptomes of several pathway genes were identified between the Delta- and Omicron-infected groups. Notably, HLA-G, previously known as potent immune-modulators that may enhance immune escape of the virus,³⁹ was significantly upregulated in Delta-infected ROIs compared to Omicron-infected ROIs. It has been reported that serum HLA-G is upregulated in severe COVID-19 patients.⁴⁰ Additionally, the role of HMGB proteins in COVID-19 pathogenesis was recently proposed, and the HMGB2 genes was selectively upregulated in Delta-infected ROIs. Recent evidence suggests that particularly HMGB1-2 may be associated with viral genome replication and inflammatory response.⁴¹ Annexin A1 (ANXA1) is an endogenous glucocorticoids that contributes to the suppression of inflammation,⁴² and the decreased serum AMXA1 levels were reported in severe/critical cases of COVID-19 disease.⁴³ Contrary to expectation, Delta-infected bronchiolar ROIs had higher expression of the ANXA1 gene. In addition, hypoxia pathway-related genes (CA12, IGFBP3, and PKP1), which have not yet been correlated with SARS-CoV-2 infection but could be potential biomarkers, were significantly upregulated in the Delta-infected ROIs. Overall, the differential expression pattern was enhanced in the large airway and

FIGURE 5 Spatial transcriptomic analysis in vascular regions of interests (ROIs) from mock-, Delta-, and Omicron-infected lungs. (A) Heat maps were illustrated for differential expression genes (DEG) obtained by comparing Q3 normalized counts between vascular ROIs in Delta- and Omicron-infected lungs versus mock-infected lungs. (B) Normalized enrichment scores (NES) and adjusted *p* values obtained by gene set enrichment analysis (GSEA) revealed vascular ROIs in Delta- and Omicron-infected lungs versus mock-infected lungs. (C) Volcano plots were shown for major differential expression genes (DEGs) between vascular ROIs of the Delta- and Omicron-infection groups. (D) Heat map of cell deconvolution data in Delta-, Omicron-, and mock-infected vascular ROIs. Results were presented for the abundance of mixed cell types in the ROIs, and scaled abundance was presented as a ratio to the max. (E) Box plots of cell deconvolution data. *****p* < 0.0001; ****p* < 0.001; ***p* < 0.01; **p* < 0.05, ANOVA, pairwise comparisons between groups, Benjamini–Hochberg FDR adjustment.

it is speculated that these transcriptional alterations during acute infection may influence the disease progression. However, it remains unclear whether the differential signature genes have a detrimental or protective role in specific microstructures. Further studies are needed on the role of each gene in the virus pathogenesis.

To build on the results of this study, conducting a follow-up study that confirms the longitudinal spatial transcriptional profiles of Delta and Omicron infections is essential. Also, the transcriptional profiling of the upper respiratory tract tissues, which exhibit varying levels of susceptibility to each variant, is needed. Given that this study was restricted to target regions with high viral load, it is necessary to validate the profiles of the two variant infections in regions with variable grades and stages of lung lesions in further investigations. In the present comparative study, we used a single strain each for Delta and Omicron infections. Various Omicron subvariants have recently emerged; thus, further studies using different strains are warranted.

To the best of our knowledge, this study represents the first attempt to uncover the pathogenesis of SARS-CoV-2 variants through a whole spatial transcriptome analysis after histopathological classification of pulmonary microstructures. A comparison of Delta- and Omicron-infected lungs revealed global pathological changes; however, the local immune response induced by the variants remained largely unchanged in lung parenchyma, with limited transcriptional alterations observed only in large airways. This study's findings can support future efforts to understand the pathogenesis of new variants and inform clinical approaches for managing immune dysregulation in SARS-CoV-2 lung infections by identifying potential transcriptional biomarkers in pulmonary microstructures.

AUTHOR CONTRIBUTIONS

Taehwan Oh conducted experiments and wrote the manuscript. Taehwan Oh, Green Kim, Seung Ho Baek, Young Min Woo, Bon-Sang Koo, Eun-Ha Hwang, Kyuyoung Shim, You Jung An, Yujin Kim, Jae-Hak Park, and Jung Joo Hong performed the experiments and managed the animals. Jung Joo Hong conceived and supervised the study.

ACKNOWLEDGMENTS

The authors thank the staff of the Korea National Primate Research Center for their excellent veterinary care. The authors also thank the staff of E-biogen Inc. (Seoul, Korea) for supporting the Nanostring GeoMx DSP platform and ExDEGA analysis software. This study was supported by the Ministry of Science and ICT of Korea under Grant NBS7952211, the Korea Research Institute of Bioscience and Biotechnology (KRIBB) Research Initiative Programs under Grant KGM4572323, and the Korea Centers for Disease Control and Prevention under Grant 2020-ER5321-00.

CONFLICT OF INTEREST STATEMENT

The authors declare no conflict of interest.

DATA AVAILABILITY STATEMENT

The datasets used and analyzed during the current study are available from the corresponding author upon reasonable request.

ETHICS STATEMENT

The study adhered to the guidelines of the US National Research Council for Laboratory Animal Care and was approved by the Korea Research Institute of Bioscience and Biotechnology (KRIBB) Institutional Animal Care and Use Committee (permit number KRIBB-AEC-22230). All procedures were conducted in a class II biosafety cabinet at the ABL-3 facility within the Korea National Primate Research Centre (KNPRC) at the KRIBB, in accordance with permit number KRIBB-IBC-20210201.

ORCID

Jung Joo Hong  <http://orcid.org/0000-0002-9795-6513>

REFERENCES

- Huang C, Wang Y, Li X, et al. Clinical features of patients infected with 2019 novel coronavirus in Wuhan, China. *Lancet*. 2020;395:497-506.
- Zhou P, Yang X-L, Wang X-G, et al. A pneumonia outbreak associated with a new coronavirus of probable bat origin. *Nature*. 2020;579:270-273.
- To KK-W, Sridhar S, Chiu KH-Y, et al. Lessons learned 1 year after SARS-CoV-2 emergence leading to COVID-19 pandemic. *Emerg Microbes Infect*. 2021;10:507-535.
- Konings F, Perkins MD, Kuhn JH, et al. SARS-CoV-2 variants of interest and concern naming scheme conducive for global discourse. *Nat Microbiol*. 2021;6:821-823.
- Menni C, Valdes AM, Polidori L, et al. Symptom prevalence, duration, and risk of hospital admission in individuals infected with SARS-CoV-2 during periods of omicron and delta variant dominance: a prospective observational study from the ZOE COVID Study. *Lancet*. 2022;399:1618-1624.
- Nyberg T, Ferguson NM, Nash SG, et al. Comparative analysis of the risks of hospitalisation and death associated with SARS-CoV-2 omicron (B.1.1.529) and delta (B.1.617.2) variants in England: a cohort study. *Lancet*. 2022;399:1303-1312.
- Uraki R, Kiso M, Iida S, et al. Characterization and antiviral susceptibility of SARS-CoV-2 Omicron BA.2. *Nature*. 2022;607:119-127.
- Suzuki R, Yamasoba D, Kimura I, et al. Attenuated fusogenicity and pathogenicity of SARS-CoV-2 Omicron variant. *Nature*. 2022;603:700-705.
- Yuan S, Ye Z-W, Liang R, et al. Pathogenicity, transmissibility, and fitness of SARS-CoV-2 Omicron in Syrian hamsters. *Science*. 2022;377:428-433.
- Chandrashekar A, Yu J, McMahan K, et al. Vaccine protection against the SARS-CoV-2 Omicron variant in macaques. *Cell*. 2022;185:1549-1555.
- van Doremalen N, Singh M, Saturday TA, et al. SARS-CoV-2 Omicron BA. 1 and BA. 2 are attenuated in rhesus macaques as compared to Delta. *Sci Adv*. 2022;8:eade1860.
- Hui KPY, Ho JCW, Cheung M, et al. SARS-CoV-2 Omicron variant replication in human bronchus and lung ex vivo. *Nature*. 2022;603:715-720.
- Hui KPY, Ng K-C, Ho JCW, et al. Replication of SARS-CoV-2 Omicron BA.2 variant in ex vivo cultures of the human upper and lower respiratory tract. *EBioMedicine*. 2022;83:104232.

14. Peacock TP, Brown JC, Zhou J, et al. The SARS-CoV-2 variant, Omicron, shows rapid replication in human primary nasal epithelial cultures and efficiently uses the endosomal route of entry. *bioRxiv*. Preprint posted online 2022. doi:10.1101/2021.12.31.474653
15. Kulasinghe A, Tan CW, Ribeiro dos Santos Miggiolaro AF, et al. Profiling of lung SARS-CoV-2 and influenza virus infection dissects virus-specific host responses and gene signatures. *Eur Respir J*. 2022;59:2101881.
16. Longo SK, Guo MG, Ji AL, Khavari PA. Integrating single-cell and spatial transcriptomics to elucidate intercellular tissue dynamics. *Nat Rev Genet*. 2021;22:627-644.
17. Delorey TM, Ziegler CGK, Heimberg G, et al. COVID-19 tissue atlases reveal SARS-CoV-2 pathology and cellular targets. *Nature*. 2021;595:107-113.
18. Desai N, Neyaz A, Szabolcs A, et al. Temporal and spatial heterogeneity of host response to SARS-CoV-2 pulmonary infection. *Nat Commun*. 2020;11:6319.
19. Koo B-S, Oh H, Kim G, et al. Transient lymphopenia and interstitial pneumonia with endotheliitis in SARS-CoV-2-infected macaques. *J Infect Dis*. 2020;222:1596-1600.
20. Baek SH, Oh H, Koo B-S, et al. Cynomolgus macaque model for COVID-19 Delta variant. *Immune Netw*. 2022;22:e45.
21. Lu M, Chamblee M, Zhang Y, et al. SARS-CoV-2 prefusion spike protein stabilized by six rather than two prolines is more potent for inducing antibodies that neutralize viral variants of concern. *Proc Natl Acad Sci*. 2022;119:e2110105119.
22. Demirkan G, Hood T, Reeves J, et al. Enabling pathway analysis of RNA expression in formalin-fixed paraffin embedded tissues with the GeoMx DSP platform. *J Biomol Tech*. 2020;31:S18.
23. Kalocsay M, Maliga Z, Nirmal AJ, et al. Multiplexed proteomics and imaging of resolving and lethal SARS-CoV-2 infection in the lung. *bioRxiv*. Preprint posted online 2020. doi:10.1101/2020.10.14.339952
24. Dinno III, KH, Leist SR, Okuda K. SARS-CoV-2 infection produces chronic pulmonary epithelial and immune cell dysfunction with fibrosis in mice. *Sci Transl Med*. 2022;14:eabo5070.
25. Danaher P, Kim Y, Nelson B, et al. Advances in mixed cell deconvolution enable quantification of cell types in spatial transcriptomic data. *Nat Commun*. 2022;13:385.
26. Rendeiro AF, Ravichandran H, Bram Y, et al. The spatial landscape of lung pathology during COVID-19 progression. *Nature*. 2021;593:564-569.
27. Park J, Foox J, Hether T, et al. Systemic tissue and cellular disruption from SARS-CoV-2 infection revealed in COVID-19 autopsies and spatial omics tissue maps. *bioRxiv*. Preprint posted online 2021. doi:10.1101/2021.03.08.434433
28. Luo W, Li Y-X, Jiang L-J, Chen Q, Wang T, Ye DW. Targeting JAK-STAT signaling to control cytokine release syndrome in COVID-19. *Trends Pharmacol Sci*. 2020;41:531-543.
29. Gupta RK, Rosenheim J, Bell LC, et al. Blood transcriptional biomarkers of acute viral infection for detection of pre-symptomatic SARS-CoV-2 infection: a nested, case-control diagnostic accuracy study. *Lancet Microbe*. 2021;2:e508-e517.
30. Mellett L, Khader SA. S100A8/A9 in COVID-19 pathogenesis: impact on clinical outcomes. *Cytokine Growth Factor Rev*. 2022;63:90-97.
31. Ziegler CGK, Miao VN, Owings AH, et al. Impaired local intrinsic immunity to SARS-CoV-2 infection in severe COVID-19. *Cell*. 2021;184:4713-4733.
32. Iwamura C, Hirahara K, Kiuchi M, et al. Elevated Myl9 reflects the Myl9-containing microthrombi in SARS-CoV-2-induced lung exudative vasculitis and predicts COVID-19 severity. *Proc Natl Acad Sci*. 2022;119:e2203437119.
33. Lan J, Ge J, Yu J, et al. Structure of the SARS-CoV-2 spike receptor-binding domain bound to the ACE2 receptor. *Nature*. 2020;581:215-220.
34. Hoffmann M, Kleine-Weber H, Schroeder S, et al. SARS-CoV-2 cell entry depends on ACE2 and TMPRSS2 and is blocked by a clinically proven protease inhibitor. *Cell*. 2020;181:271-280.
35. Qiao J, Li W, Bao J, et al. The expression of SARS-CoV-2 receptor ACE2 and CD147, and protease TMPRSS2 in human and mouse brain cells and mouse brain tissues. *Biochem Biophys Res Commun*. 2020;533:867-871.
36. Wang K, Chen W, Zhou Y-S, et al. SARS-CoV-2 invades host cells via a novel route: CD147-spike protein. *bioRxiv*. Preprint posted online 2020. doi:10.1101/2020.03.14.988345
37. Crawley JTB, Goulding DA, Ferreira V, Severs NJ, Lupu F. Expression and localization of tissue factor pathway inhibitor-2 in normal and atherosclerotic human vessels. *Arterioscler Thromb Vasc Biol*. 2002;22:218-224.
38. Giannis D, Ziogas IA, Gianni P. Coagulation disorders in coronavirus infected patients: COVID-19, SARS-CoV-1, MERS-CoV and lessons from the past. *J Clin Virol*. 2020;127:104362.
39. Lin A, Yan WH. Perspective of HLA-G induced immunosuppression in SARS-CoV-2 infection. *Front Immunol*. 2021;12:5192.
40. Al-Bayate NT, Ad'hiah AH. Soluble HLA-G is upregulated in serum of patients with severe COVID-19. *Hum Immunol*. 2021;82:726-732.
41. Islam MT, Hossen M, Kamaz Z, et al. The role of HMGB1 in the immune response to SARS-CoV-2 infection: from pathogenesis towards a new potential therapeutic target. *Farmacia*. 2021;69:621-634.
42. Sugimoto MA, Vago JP, Teixeira MM, Sousa LP. Annexin A1 and the resolution of inflammation: modulation of neutrophil recruitment, apoptosis, and clearance. *J Immunol Res*. 2016;2016:1-13.
43. Canacik O, Sabirli R, Altintas E, et al. Annexin A1 as a potential prognostic biomarker for COVID-19 disease: case-control study. *Int J Clin Pract*. 2021;75:e14606.

SUPPORTING INFORMATION

Additional supporting information can be found online in the Supporting Information section at the end of this article.

How to cite this article: Oh T, Kim G, Baek SH, et al. Comparative spatial transcriptomic profiling of severe acute respiratory syndrome coronavirus 2 Delta and Omicron variants infections in the lungs of cynomolgus macaques. *J Med Virol*. 2023;95:e28847. doi:10.1002/jmv.28847